Initiation Mechanism of Peeling in Rolling Bearings, and Its Life Estimation Method

Naoya HASEGAWA*
Takumi FUJITA*
Michimasa UCHIDATE**
Masayoshi ABO***
Hiroshi KINOSHITA***

Peeling, which consists of spalls and cracks of about 10 μm in size, is one of the common failure modes of rolling bearings. Peeling is known to occur under poor lubrication conditions which result in direct contact of surface roughness asperities. However, the initiation mechanism of peeling is not yet completely understood. In this study, we investigated the peeling formation mechanism by observation of rolling contact surfaces, surface topography measurements, residual stress measurements, and contact analysis. These results clarified that initial peeling cracks arose from notches which formed due to plastic contact of surface roughness asperities.

We also developed a peeling life estimation method based on the above formation mechanism. The method can estimate peeling life under pure rolling and boundary lubrication conditions.

1. Introduction

In order to reduce friction, the recent trend has been towards the use of low viscosity oil lubrication. The chance that rolling bearings (hereafter, "bearings") are used in thin lubricating conditions is therefore increasing. Thus, clarifying the damage mechanism of bearings under such conditions has become an important engineering task.

Peeling is one type of failure experienced by bearings operating under thin lubricating conditions and is indicated by dense area of spalls and cracks approximately 10 μm in size[1]. Peeling is likely to occur when the surface roughness is high and the oil film parameter Λ (ratio between the minimum oil film thickness obtained from the EHL Theory and the square root of the square sum of the root-mean-square roughness of two surfaces) is low[2]. Therefore, repeated stress applied on the direct contact area (hereafter, "real contact area") of the surface roughness is the cause of peeling. Although, the peeling mechanism is roughly understood, the details remain unclear[3) 4)]. The authors studied the formation mechanism of peeling in detail by reproducing peeling with a two-cylinder type testing machine, observing the rolling contact surface, and conducting various analyses[5]. In addition, the mechanism of crack formation during peeling was quantitatively examined by estimating the repeated stress applied to the real contact area using the surface topography and the measurement of residual stress[6]. Chapter 2 of this paper explains the peeling formation mechanism obtained from this study.

In order to examine the reliability of bearings under thin lubricating conditions, a tool to estimate peeling life is also required. The authors developed a life estimation method based on the above peeling mechanism[7]. Chapter 3 of this paper describes this method for estimating peeling life.

2. Peeling formation mechanism

2.1 Two-cylinder test

The two-cylinder type tester shown in **Fig. 1** was used to reproduce peeling. A driving cylinder attached to a motor is put in contact with a driven cylinder, both of which are rotated under a pure rolling condition without slippage. Lubrication was provided through an oil saturated felt pad in contact with the test pieces. The test pieces were both 40 mm OD and 12 mm in length, with a 60 mm crown radius placed axially along the outer diameter surface of the driving cylinder. The material of the test pieces is JIS-SUJ2 with ordinary quenching and tempering. A ground finish was applied to the outer diameter of the driving cylinder while superfinishing was applied to the driven cylinder. Two types of driving cylinders were prepared, one with black oxide treatment (Test No. 2) and the other without such treatment (Test No. 1). The purpose is to examine how the reduction of surface roughness (hereafter, "running-in")[8] progresses due to black oxide treatment affects the formation of peeling. The condition of the black oxide treatment was set based on DIN 50938[9]. **Table 1** shows the surface roughness, hardness and thickness of the black oxide layer and **Table 2** shows the test conditions. The test was interrupted after each loading cycle, with analysis to be described later taking place, then the test continued until the total number of loading cycles reached 5.0×10^5.

* Advanced Technology R&D Center
** Faculty of Science and Engineering, Iwate University
*** School of Engineering, University of Hyogo

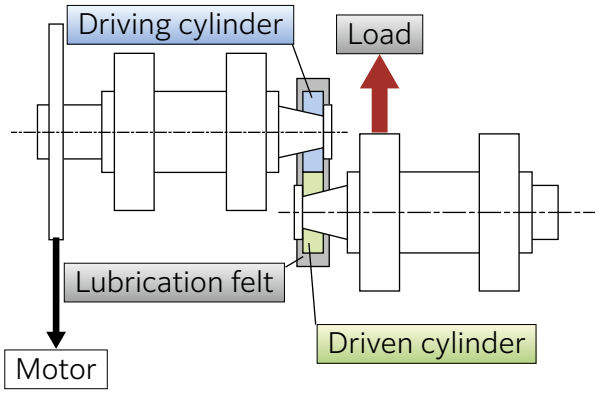

Fig. 1 Two-cylinder type rolling contact fatigue tester

2.2 Observation of rolling contact surface, measurement of shape and analysis of surface roughness

Under the conditions shown in **Table 1**, peeling is likely to form on the driven cylinder with lower surface roughness. Therefore, peeling formation was examined by observing the rolling contact surface of the driven cylinder with an optical microscope and scanning electron microscope (hereafter, "SEM"). For observation of the crack section of peeling, a focused ion beam (FIB) system was used to prepare the test pieces.

Topography of the rolling contact surface of both cylinders was measured by confocal laser scanning microscopy and used in the estimation of repetitive stress on the rolling contact surface, as described later. In addition, the relationship between the change of surface topography on the driven cylinder and formation of peeling was investigated. Furthermore, to study the relationship between the degree of running-in and the formation of peeling, two types of 3-dimensional roughness parameters on the surface topography of the driving cylinder (standard deviation σ^* of height of protrusions and arithmetic mean curvature S_{pc}) were analyzed. Based on the theory of rough surface contact of Greenwood, etc.[10], the severity of contact at the real contact area decreases as the product of σ^* and S_{pc} ($\sigma^* \cdot S_{pc}$) is reduced. In section 2.5.2, the relationship between $\sigma^* \cdot S_{pc}$ and the progress of peeling will be discussed.

2.3 Estimation of repeated stress of rolling contact surface

Triaxial stress components of contact stress that act on the real contact area were estimated during the test by elastic analysis using the boundary element method[11]. In this analysis, the oil film parameter during the test was low ($\Lambda \approx 0.10$), so we assumed there was no load supported by the oil film. The subject area of the analysis was set to the area surrounding the center of the contact ellipse where the apparent contact pressure is relatively large. The details of the analysis are discussed in reference 6).

Furthermore, under the condition that the oil film parameter is low, plastic deformation occurs in the contact region and residual stress is produced on the rolling contact surface. In this study, triaxial stress components of the residual stress on the driven cylinder were measured with the X-ray stress measuring method[12] and the area detector method.

The triaxial stress components that actually acted on the rolling contact surface can be estimated with the following equation (1) by adding the results from the above contact analysis and X-ray stress measurement.

$$\hat{\sigma} = \sigma_{con} + \sigma_{res} \quad (1)$$

Where, the subscripts 'con' and 'res' indicate contact stress and residual stress, respectively. As discussed later, plastic deformation of the rolling contact surface is involved in the formation of the initial cracks in peeling. Therefore, in the study of the formation mechanism of peeling, the discussion uses von Mises stress (hereafter, "Mises stress") which indicates the yield condition of the material. Mises stress σ_{vm} can be obtained by the following equation (2) by using the triaxial stress components obtained in equation (1).

$$\sigma_{vm} = \sqrt{\frac{1}{2}\left\{(\sigma_x - \sigma_y)^2 + (\sigma_y - \sigma_z)^2 + (\sigma_z - \sigma_x)^2 + 6(\tau_{xy}^2 + \tau_{yz}^2 + \tau_{zx}^2)\right\}} \quad (2)$$

Table 1 Surface roughness, hardness and thickness of the black oxide layer for test cylinders

Test No.	Surface roughness (R_a) μm		Hardness		Thickness of black oxide layer μm	
	Driving cylinder	Driven cylinder	Driving cylinder	Driven cylinder	Driving cylinder	Driven cylinder
1	0.75	0.02	61.5 HRC		-	-
2	0.70				2.0	

Table 2 Test conditions of the RCF testing

Items	Conditions
Lubricant	poly- α -olefin, VG5
Rotational speed min^{-1}	2,000
Load kN	2.25
Maximum contact pressure GPa	2.3
Oil film parameter Λ	0.09 - 0.11 (at 40 ℃)
Total number of loading cycles	5.0×10^5

2.4 Results of experiment and analysis

2.4.1 Observation of rolling contact surface of the driven cylinder

Fig. 2 shows optical micrographs of the rolling contact surface on the driven cylinder. Test No. 1 shows crack-like damage at 0.1×10^5 loading cycles. At 2.5×10^5 loading cycles, the damage increased, then at the 5.0×10^5 cycles, several small spalls approximately 10 μm in size are also observed. On the other hand, no damage formed on No. 2 even after 5.0×10^5 loading cycles.

Fig. 3 shows the topography of the rolling contact surface on the driven cylinder. **Fig. 3** (a) shows the pre-test surface topography created by superfinishing. In **Fig. 3** (b) Test No. 1 at the 1.0×10^5 loading cycles, the wavy pattern indicates a larger amplitude and period than before the test, as well as multiple small protrusions. These protrusions matched the location of the damage seen in **Fig. 2** (b). On the other hand, **Fig. 3** (c) Test No. 2 at 1.0×10^5 loading cycles shows a wavy pattern, however, its amplitude is small and no small protrusions are observed.

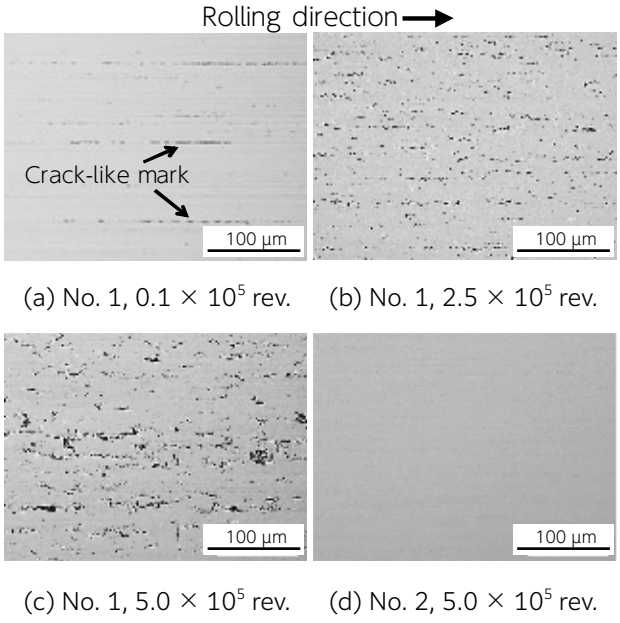

(a) No. 1, 0.1×10^5 rev. (b) No. 1, 2.5×10^5 rev.

(c) No. 1, 5.0×10^5 rev. (d) No. 2, 5.0×10^5 rev.

Fig. 2 Optical micrographs of rolling contact surfaces for driven cylinders

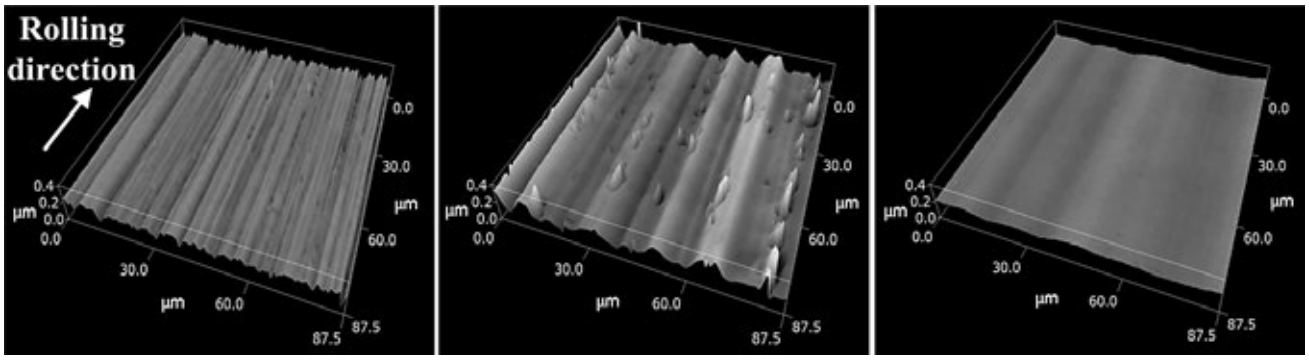

(a) No. 1, Before testing (b) No. 1, 1.0×10^5 rev. (c) No. 2, 1.0×10^5 rev.

Fig. 3 Surface topographies of driven cylinders measured by laser microscopy

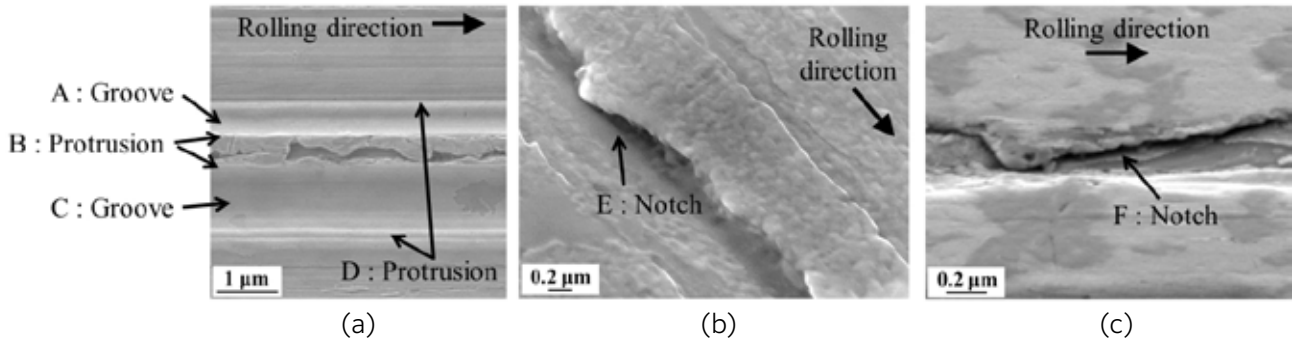

Fig. 4 SEM images of the crack-like marks on the driven cylinder of test No. 1 at 0.1 × 10^5 rev.

Fig. 4 shows the damage seen on the Test No. 1 driven cylinder at 0.1 × 10^5 loading cycles observed by SEM. **Fig. 4** (a) - (c) show higher magnification views from different observation points. In **Fig. 4** (a), protruded areas (B and D in the figure) exist adjacent to grooves on both sides (A and C in the figure). This means the aforementioned wavy pattern was formed by plastic deformation. In **Fig. 4** (b), the protruded area of the wave is deformed as if pressed in the vertical direction, from which a notch (E in the figure) was formed. A notch (F in the figure) was also formed in **Fig. 4** (c), however, it was folded down along the slope of the adjacent groove.

Fig. 5 shows the damage on the Test No. 1 driven cylinder at 5.0 × 10^5 loading cycles observed by SEM from the axial direction. A crack which propagated from the notch (area enclosed by dotted line in the figure) can be seen.

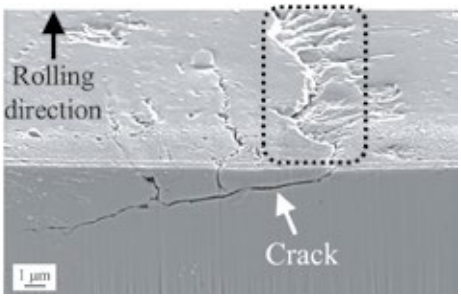

Fig. 5 Cross-section SEM image of the crack-like mark on the driven cylinder of test No. 1 at 5.0 × 10^5 rev.

2.4.2 Measurement result of residual stress

Fig. 6 shows the relationship between the residual stress on the rolling contact surface of the driven cylinder and number of loading cycles. The value of the vertical axis $\sigma_{vm,res}$ is the Mises stress calculated from the triaxial stress components. The inserted graph in the figure is an enlarged view during the early loading cycles. $\sigma_{vm,res}$ of Tests No. 1 and No. 2 stabilized at 1,050 - 1,100 MPa after 0.1 × 10^5 loading cyles.

The rate of increase of $\sigma_{vm,res}$ was slightly slower for No. 2. **Table 3** shows the triaxial stress components of the residual stress of the driven cylinder at 0.5 × 10^5 loading cycles, at which point there was almost no difference in residual stress between Tests No. 1 and No. 2.

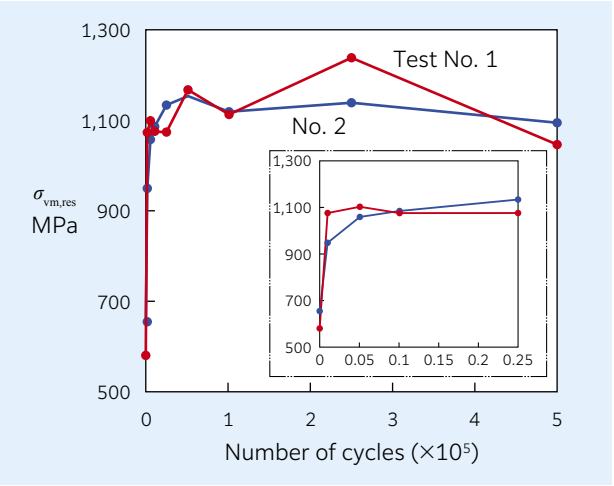

Fig. 6 Relationship between residual stresses at rolling contact surfaces of driven cylinders and loading cycles

Table 3 Tri-axial stress components of residual stresses for driven cylinders at 0.5 × 10^5 rev.

Test No.	Residual stress GPa					
	σ_x	σ_y	σ_z	τ_{xy}	τ_{yz}	τ_{zx}
1	-1.53	-1.34	-0.37	-0.02	-0.01	0.00
2	-1.52	-1.43	-0.41	-0.01	0.02	0.00

2.4.3 Surface roughness parameters of driving cylinder

Fig. 7 shows the relationship between the surface roughness of the driving cylinder and the loading cycles. In each test, $\sigma^* \cdot S_{pc}$ decreased immediately after the start of testing, however, Test No. 2 decreased more than Test No. 1. This means that the

severity of contact due to running-in is much lower in Test No. 2 when compared to Test No. 1.

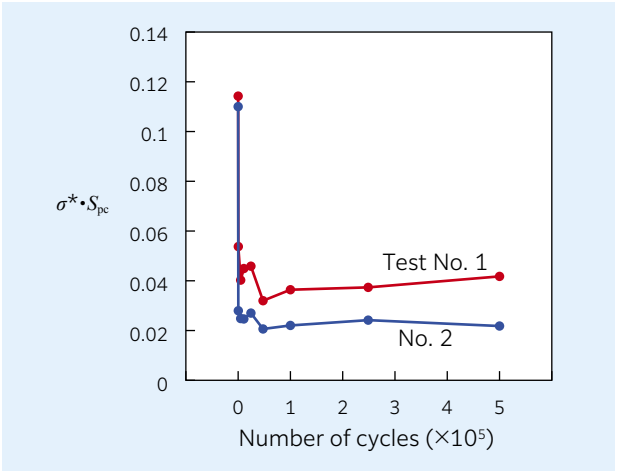

Fig. 7 Relationship between the surface roughness of driving cylinders and loading cycles
(σ^* : Standard deviation of peak height, S_{pc} : Arithmetic mean peak curvature)

2.4.4 Estimation result of repeated stress applied to rolling contact surface

Fig. 8 shows the pressure distribution of the real contact area on the rolling contact surface obtained by contact analysis. On the rolling contact surface of Tests No. 1 and No. 2 before testing, contact pressure of more than 10 GPa was observed. Areas of more than 10 GPa were found on Test No. 1 at 0.5×10^5 loading cycles, however most areas on the rolling contact surface were less than 10 GPa for Test No. 2.

Fig. 9 shows the distribution of Mises stress acting on the rolling contact surface of the driven cylinder, in the depth direction, at 0.5×10^5 loading cycles. In the figure, Mises stress that considered the residual stress $\overline{\hat{\sigma}_{vm}(z)}$ and Mises stress that did not consider residual stress $\sigma_{vm,\,con}(z)$ are both plotted. The stress values on the vertical axis indicate the mean values of Mises stresses at points where the stresses are the largest among the neighboring stress values (within a square area of 6.25 μm centered on the own points) on the x-y plane of depth z. The area enclosed by a dotted line in the figure shows the yield stress of the bearing steel (1.8 - 2.0 GPa[13]). $\overline{\hat{\sigma}_{vm}(z)}$ in Tests No. 1 and No. 2 exceeded the yield stress in all the areas up to 5 μm of depth. $\overline{\hat{\sigma}_{vm}(z)}$ in Test No. 2 was smaller than Test No. 1 at all depths. In addition, the maximum value of $\overline{\hat{\sigma}_{vm}(z)}$ occurred at about 0.5 μm for both tests. The stress value for Test No. 2 at this depth was about 40 % smaller than for Test No.1. In all tests, $\overline{\hat{\sigma}_{vm}(0.5)}$ was about 10 % smaller than $\sigma_{vm,\,con}(0.5)$.

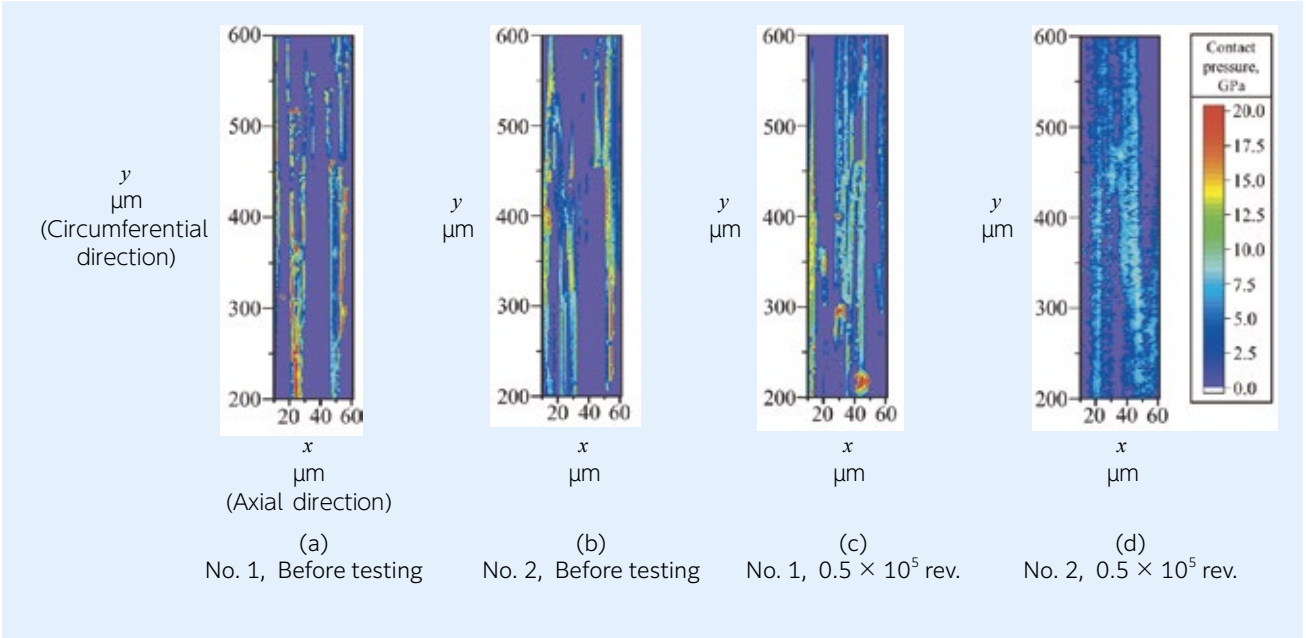

Fig. 8 Contact pressure distributions at real contact area on rolling contact surfaces

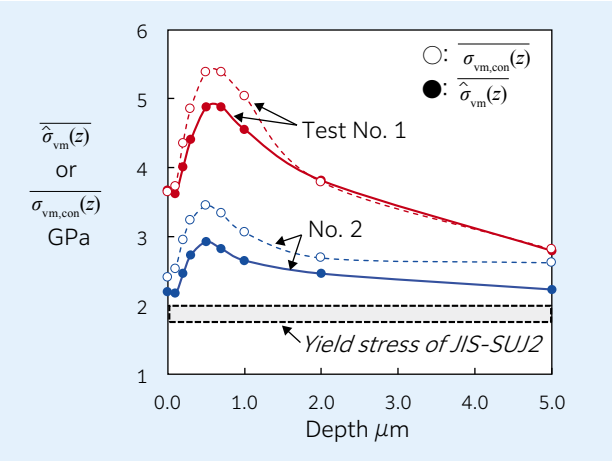

Fig. 9 Depth dependence of von Mises stress on the rolling contact surface of the driven cylinder at 0.5×10^5 rev.

2.5. Discussion

2.5.1 Crack formation mechanism in peeling

From observation with the optical microscope in **Fig. 2**, small peeling spalls formed on the driven cylinder in Test No. 1 which seem to be a result of propagation of the damage that initiated from small cracks at 2.5×10^5 loading cycles (hereafter, "initial cracks"). Also, it is assumed that the initial cracks were formed from micro-scaled plastic deformation originating on the driven cylinder during rotation, based on measurement of the surface shape in **Fig. 3** and observation by SEM in **Fig. 4**. Based on these results, **Fig. 10** shows a schematic diagram of the formation mechanism of peeling cracks. Initially, asperity on the rough surface of the driving cylinder contacts the rolling contact surface of the driven cylinder, which creates a wrinkle-like pattern of plastic deformation on the driven cylinder (Steps 1-2). Subsequent asperities, contact the plastically deformed surface of the driven cylinder, flattening the protrusions. Additional rolling creates notch folding which leads to stress concentrations and initial cracking (Steps 3-4). A similar phenomenon is also observed in a study of micro-pitting of gears by Mallipeddi, etc[14]. Based on the above mechanism, it can be assumed that the risk of peeling crack formation will be larger when plastic deformation on the rolling contact surface is high. In fact, the plastic deformation of the driven cylinder in Test No. 1, where peeling formed, was more significant than on the driven cylinder of Test No. 2 where peeling did not form.

2.5.2 Relationship between repeated stress of rolling contact surface and peeling formation

It is assumed that a stress of $\overline{\hat{\sigma}_{vm}(z)}$ over the yield stress was applied to the driven cylinders in Tests No. 1 and No. 2 and plastic deformation continued even after "running-in" and stabilization of residual stress (after 0.5×10^5 loading cycles) . It is also understood that the plastic deformation of the driven cylinder was more significant on Test No. 1 than Test No. 2 because $\overline{\hat{\sigma}_{vm}(z)}$ up to 5 μm of depth was larger . From the above, it seems that peeling life (formation of initial cracks and degree of progress) should be shorter as the repeated stress on the rolling contact surface is larger and the degree of plastic deformation is greater.

Both cylinders in Tests No. 1 and No. 2, $\overline{\hat{\sigma}_{vm}(z)}$ was approximately 10 % smaller than $\sigma_{vm,\,con}(z)$ at the same depth. This indicates that the Mises stress acting on the rolling contact surface was reduced due to the impact of the residual stress, so the residual stress must affect the peeling life. However, as shown in **Table 3**, there was no difference between the residual stresses in Tests No. 1 and No. 2, so the impact of residual stress was not apparent.

In test No. 2 where black oxide treatment was applied to the driving cylinder, the Mises stress acting upon the rolling contact surface at 0.5×10^5 loading cycles was smaller than No. 1. This is due to the lower $\sigma^* \cdot S_{pc}$ on the driving cylinder in Test No. 2, indicating better "running-in", was the main reason that peeling did not occur on the driven cylinder in Test No. 2.

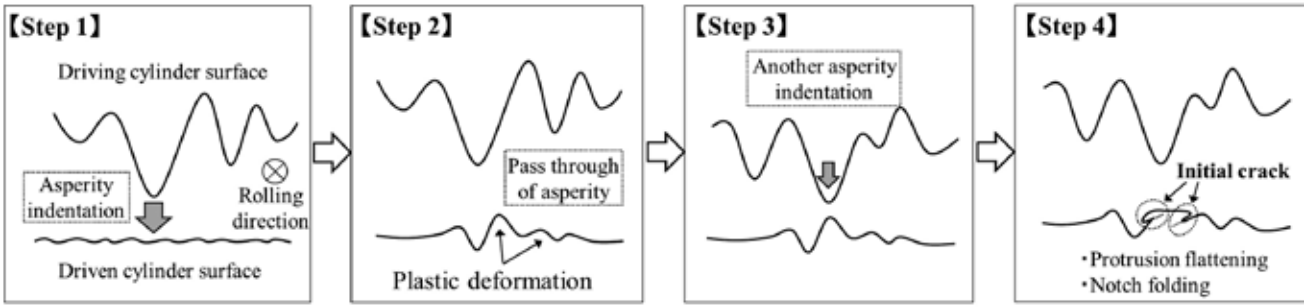

Fig. 10 Formation mechanism of a crack in peeling on the driven cylinder

3. Development of peeling life estimation

3.1 Overview of life estimation method

We have developed a peeling life estimation method based on the findings of the mechanism described in Chapter 2[7]. **Fig. 11** shows an overview of the life estimation method. First, conduct rolling contact fatigue tests under various operating conditions to obtain a peeling life and a history of repeated stresses acting on the rolling contact surface. (hereafter, "stress history") for each test (Step 1). The stress history changes depending on running-in and change of residual stress. Therefore, estimation must be done based on the contact analysis using the actual measured surface topography and residual stress measurement. Then, obtain peeling *S-N* curves (Stress – Number of cycles to failure) by regression analysis by applying Miner's rule to the data obtained in Step 1 (Step 2). Finally, estimate the peeling life under any conditions using this *S-N* curve. At this time, conduct a preliminary test simulating operating conditions of the subject of estimation, obtain stress history under those conditions (Step 3) and estimate the life using the *S-N* curve from the obtained stress history and Miner's rule (Step 4). *S-N* curves must be prepared for each steel type and thermal treatment of the rolling elements. The preliminary tests can be conducted up to the loading cycles where running-in and residual stress become stable. In our experience, running-in and residual stress stabilize by 10^4 loading cycles, under the condition that the oil film parameter is lower than 1.5.

Currently, it is difficult to accurately simulate running-in and change in residual stress of rolling elements used in various conditions. In this estimation method, the impact of running-in and change of residual stress can be considered based on preliminary test that simulates the actual operating conditions. Impact of the materials can also be considered if *S-N* curves for each steel type and thermal treatment are prepared.

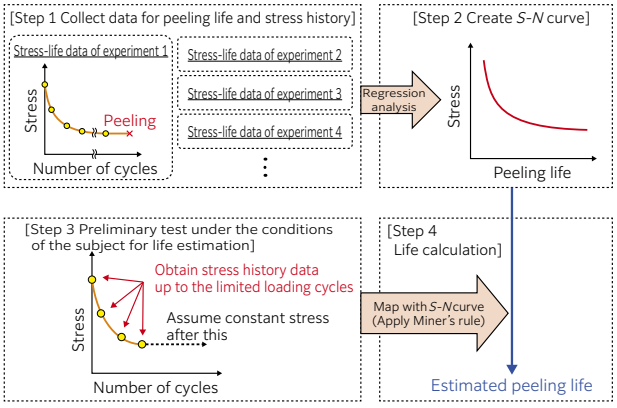

Fig. 11 Flow of the estimation method of peeling life

3.2 Various assumptions for this life estimation method

It must be noted that the following are assumed in this life estimation method.

1) Repeated stress that produces peeling (dominant stress) is Mises stress.
2) The relationship between peeling life and repeated stress follows Miner's rule.
3) Loss of fatigue layer of the surface layer due to wear is negligible.
4) The relationship between peeling life L_{th} and repeated stress $\overline{\hat{\sigma}_{vm}(z)}$ can be expressed by the *S-N* curve of the double logarithmic model in the following equation (3).

$$\log L_{th} = -A \log (\overline{\hat{\sigma}_{vm}(z)} - S_f) + \log B \quad (3)$$

Where, A, B and S_f are constants specific to the materials.

Using Mises stress as the dominant stress of peeling in 1) should be appropriate considering that formation of peeling is affected by the magnitude of plastic deformation of the rolling contact surface. Use of Miner's rule and the *S-N* curve of the double logarithmic model in 2) and 4) is generally adopted in other research involving rolling fatigue life estimation[15) 16)] and this method also followed that practice. The assumption of 3) impact of wear, should be considered appropriate under the conditions that the depth of wear on the rolling contact surface is relatively small. It should be noted that the scope of application of this life estimation method is currently limited to pure rolling and boundary lubrication conditions.

3.3 Validation of life estimation accuracy

The accuracy of this life estimation method was examined by conducting two - cylinder type tests similar to **Fig. 1** under various test conditions. **Table 4** shows the test conditions and **Fig. 12** shows the relationship between the estimated peeling life (L_{est}) and the actual life (L_{act}). *S-N* curves were generated with the test data from Test No. 1 - 7 and the estimated life of each test was obtained from the stress history of up to 10^4 cycles. In the figure, the median, minimum and maximum values of the life ratio (L_{act}/L_{est}) are indicated. These statistics values within the range of this test condition was 0.89, 0.49 and 1.82, respectively. This accuracy is the same or higher than other life estimation methods[17)] (90 % reliability interval of L_{act}/L_{est} under thin lubrication condition is 0.98-4.3), therefore, this life estimation method should be applicable as one of the peeling life estimation methods. The tests of No. 8 and No. 9 were additionally conducted after generating the *S-N* curves. The life ratios of these tests were 0.61 and 1.07, respectively, thus, the validated life estimate of the same accuracy as those in Test No. 1 - 7.

Moving forward, we plan to develop methods applicable to conditions with slippage and mixed lubrication, in order to expand the scope and application of this life estimation method.

Table 4 Test conditions of the RCF testing for validation of the life estimation accuracy

Test No.	Surface roughness (R_a) μm		Rotational speed min^{-1}	Maximum contact Pressure GPa	Oil film parameter Λ
	Driving cylinder	Driven cylinder			
1	0.75	0.02	2,000	2.3	0.11
2	0.40				0.21
3	0.35				0.24
4	0.30				0.28
5	0.75		500		0.06
6	0.75		2,000	1.6	0.12
7	0.40		1,000	2.3	0.17
8	0.50		2,000		0.17
9	0.75				0.11

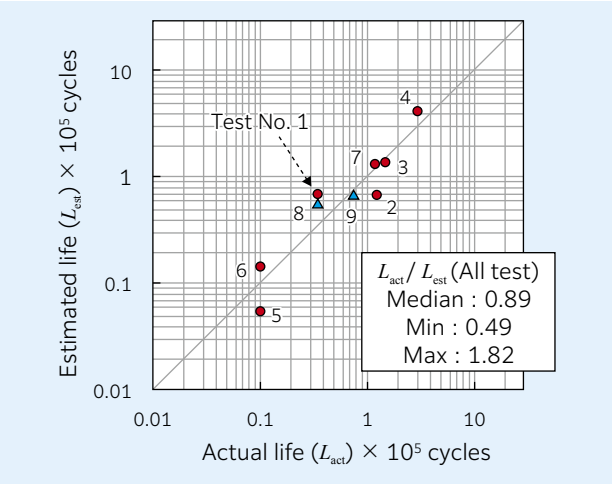

Fig. 12 Relationship between estimated peeling lives and actual peeling lives

4. Summary

In this paper, we examined the formation mechanism of peeling based on experiments and analysis. We also introduced a life estimation method based on the peeling formation mechanism.

1) Initial peeling cracks are produced from the notches which are formed by plastic deformation of protrusions on the rolling contact surface.
2) The developed life estimation method can estimate peeling life under pure rolling and boundary lubrication conditions with the same or better accuracy than other life estimation methods. Moving forward, we also plan to develop life estimation methods applicable to conditions with slippage and mixed lubrication.

This paper is a compilation of 2 papers published in "The Tribologist," the Journal of the Japanese Society of Tribologists, Vol. 63, Issue 8 (2018) 551 and Issue 9, (2018) 618, "Mechanism for Initiation of Peeling in Rolling Contact and the Effect of Black Oxide Treatment on the Suppression of Peeling (Part 1 and 2)" and another paper published in its English Journal, "Tribology Online" Vol. 14, Issue 3 (2019) 131, "Estimation Method of Micropitting Life from *S-N* Curve Established by Residual Stress Measurements and Numerical Contact Analysis." We appreciate generosity of the Japanese Society of Tribologists, who permitted this publication.

References

1) Noriyuki Tsushima, Hirokazu Nakashima, Hiroshi Kashimura, Typical Failures of Bearings, NTN TECHNICAL REVIEW, No. 57 (1990) 59.
2) Y. Akamatsu, et. al., SAE Paper, 891909, (1989).
3) K. Maeda, N. Tsushima & H. Muro, The Inclination of Cracking in the Peeling Failure of a Ball Bearing Steel and its Relationship to the Inclination of the Principal Residual Stress, Wear, 65, (1980) 175.
4) A. Oila, B. A. Shaw, C. J. Aylott & S. J. Bull, Martensite Decay in Micropitted Gears, Proc. IMechE. Part J. J. Eng. Trib., 219, (2005) 77.
5) Naoya Hasegawa, Takumi Fujita, Michimasa Uchidate, Masayoshi Abo, Mechanism for Initiation of Peeling in Rolling Contact and the Effect of Black Oxide Treatment on the Suppression of Peeling (Part 1), The Tribologist, 63, 8, (2018) 551.
6) Naoya Hasegawa, Takumi Fujita, Michimasa Uchidate, Masayoshi Abo, Mechanism for Initiation of Peeling in Rolling Contact and the Effect of Black Oxide Treatment on the Suppression of Peeling (Part 2), The Tribologist, 63, 9, (2018) 618.
7) N. Hasegawa. T. Fujita, M. Uchidate, M. Abo & H. Kinoshita, Estimation Method of Micropitting Life from *S-N* Curve Established by Residual Stress Measurements and Numerical Contact Analysis, Tribology Online, 14, 3, (2019) 131.
8) V. Brizmer, K. Sradler, M. V. Drogen, B. Han, C. Matta & E. Piras, The Tribological Performance of Black Oxide Coating in Rolling/Sliding Contacts, STLE Tribol. Trans., 60, 3, (2017) 557.
9) DIN 50938, (2003).
10) J. A. Greenwood & J. B. P. Williamson, Contact of Nominally Flat Surfaces, Proc. Roy. Soc. London, A295, (1966) 300.
11) M. Uchidate, Comparison of Contact Conditions Obtained by Direct Simulation with Statistical Analysis for Normally Distributed Isotropic Surfaces, Surface Topography, Metrology and Properties, 6, 3, (2018) 034003.
12) Toshihiko Sasaki, Shun-ichi Takahashi, Katsunari Sasaki, Yuichi Kobayashi, A Study on Improvements in Multiaxial Stress Analysis with Area Detector Type Diffraction Method, Transactions Vol. A of The Japan Society of Mechanical Engineers, 75, 750 (2009) 219.
13) E. Yhland, Static Load-Carrying Capacity, Ball Bearing Journal, SKF, 211, (1982) 1.
14) D. Mallipeddi, M. Norell, M. Sosa & L. Nyborg, Influence of running-in on surface characteristics of efficiency tested ground gears, Tribology Int., 115, (2017) 45.
15) L. Houpert & F. Chevalier, Rolling Bearing Stress Based Life-Part I, Calculation Model, Journal of Tribology, 134, 2, (2012) 021103, 1.
16) S. Shimizu, Fatigue Limit Concept and Life Prediction Model for Rolling Contact Machine Elements, Tribology Transactions, 45, 1, (2002) 39.
17) J.Gnagy, L. Houpert & F. Chevalier, Rolling Bearing Stress Based Life-Part II, Experimental Calibration and Validation, Journal of Tribology, 134, 2, (2012) 021104, 1.

Photo of authors

Naoya HASEGAWA
Advanced Technology R&D Center

Takumi FUJITA
Advanced Technology R&D Center

Michimasa UCHIDATE
Faculty of Science and Engineering, Iwate University

Masayoshi ABO
School of Engineering, University of Hyogo

Hiroshi KINOSHITA
School of Engineering, University of Hyogo